THE JOURNAL OF CHEMICAL PHYSICS **131**, 144903 (2009)

Correlation between structure and rheology of a model colloidal glass

E. Di Cola,[1] A. Moussaïd,[1] M. Sztucki,[1] T. Narayanan,[1,a] and E. Zaccarelli[2]
[1]*European Synchrotron Radiation Facility, BP 220, 38043 Grenoble, France*
[2]*Dipartimento di Fisica and CNR-INFM-SOFT, Universitá di Roma La Sapienza, Piazzale A. Moro 2, I-00185 Rome, Italy*

(Received 18 June 2009; accepted 8 September 2009; published online 13 October 2009)

The microstructure and rheological properties of a model colloidal system was probed in the vicinity of the glass transition by small-angle and ultra small-angle x-ray scattering, dynamic light scattering (DLS) and bulk rheology. The volume fraction of the particles was deduced by modeling the structure factor and the absolute scattered intensity in a self-consistent way. The glass transition (ϕ_G) was identified from the frequency dependence of the shear moduli in the linear regime. The experimentally observed behavior was then compared with the viscoelastic properties derived from mode-coupling theory (MCT) using the experimental structure factor as input to the theory. The ensemble-averaged intermediate scattering functions from DLS measurements were also compared with those calculated from the MCT and reasonable agreement was obtained. © *2009 American Institute of Physics*. [doi:10.1063/1.3240345]

I. INTRODUCTION

Colloidal suspensions have been widely used to mimic supercooled liquid and glass transition in hard-sphere (HS) systems.[1–4] In a HS repulsive system, the glass transition at high packing densities corresponds to the trapping of each particle by the cage formed by its nearest neighbors.[5,6] The addition of a short-ranged attraction leads to a different glass scenario, namely, the attractive glass, and these arrested states have been an active area of research over the last decade.[7–13] In general, a good agreement between experimental observations and predictions by mode-coupling theory (MCT) as well as computer simulations has been obtained.[14–19] Nevertheless, one-to-one correspondence between the experimental microstructure and dynamical properties predicted by MCT is lacking to date. Therefore, the understanding of colloidal glassy structure and dynamics is still incomplete.

Experimentally, there are three major bottlenecks: (I) the exact separation of the structure factor from the measured intensity is still a challenging task; (II) for moderate polydispersities, the volume fraction of the particles is difficult to obtain; (III) accurate dynamic measurements are not easy due to nonergodicity, aging, and the presence of heterogeneities in the samples. From a fundamental point of view, the dynamics of colloidal dispersions differ from those of atomic systems in two respects. First, the short-time motion is diffusive rather than ballistic. Second, hydrodynamic interactions couple the motions of different particles in a complicated and subtle way.

The purpose of this article is to probe the microstructure and rheology of model colloidal glasses quantitatively and to compare the derived viscoelastic properties with the predictions by MCT using the experimental structure factor as input to the theory. For HS colloidal glasses, the main control parameter is the packing or volume fraction (ϕ) of the particles assuming that the finite polydispersity of the particles has a less critical influence on the glass transition. However, experimentally ϕ is often uncertain at the required precision. Here, we have determined the effective ϕ using the absolute scattered intensity and known mass density of particles together with the modeling of the structure factor in a self-consistent way.

In this work, we used the model colloidal system poly-(methyl methacrylate) particles (PMMA) in *cis*-decaline. We have determined the structure factor of interparticle interactions using high resolution small-angle and ultra small-angle x-ray scattering (SAXS and USAXS, respectively), particle dynamics by dynamic light scattering (DLS) and viscoelastic properties from stress-controlled rheology. As mentioned before, the experimental structure factors were used as input to the MCT calculations to predict the corresponding intermediate scattering function and rheological properties.

II. EXPERIMENTAL

A. Material

Colloidal particles consisted of PMMA core stabilized by a thin layer (~10 nm) of poly(hydroxystearic) acid (PHSA) and suspended in *cis*-decaline (Sigma-Aldrich).[1] The size of the particles was measured by SAXS with a dilute suspension. The volume fraction (ϕ) of the suspensions was estimated from the structure factor measured by means of USAXS and from the absolute intensity scale.

B. SAXS and USAXS

USAXS measurements were performed at the High Brilliance beam line (ID2), European Synchrotron Radiation Facility in Grenoble (France), using a Bonse–Hart camera.[20] The crossed analyzer configuration in the setup permitted to obtain intensity profiles, $I(q)$, directly in absolute scale,

---

[a] Electronic mail: narayan@esrf.eu.

without any smearing. Typical USAXS scans provide a useful q range of $10^{-3}\ \mathrm{nm}^{-1} \leq q \leq 0.2\ \mathrm{nm}^{-1}$, where $q = 4\pi/\lambda_0 \sin(\theta/2)$, θ being the scattering angle. The incident x-ray wavelength (λ_0) was 0.1 nm in all the experiments. The samples were loaded in thin walled flat glass capillaries with 0.5 or 1 mm thickness. Additional SAXS measurements were made using the pinhole camera, with 10 m sample to detector distance, corresponding to a q range between 0.01 and 0.3 nm^{-1}. The scattering form factor was measured using a flow through capillary of ~2 mm diameter, where the sample and solvent scattering can be measured at the same place allowing very reliable subtraction of the background. Both SAXS and USAXS measurements were performed at a temperature of 20 °C.

C. Rheology

High resolution rheology was carried out using a stress-controlled rheometer (Haake, RS300 equipped with microtorque option) having a plate-plate geometry, thermostated to ±0.01 °C. For the rheology experiments, the suspensions of PMMA particles were homogenized at ambient temperature and then transferred to the plates maintained at 18 °C in order to minimize solvent evaporation. The thickness of the sample was 0.5 mm and special care was paid in the determination of the diameter of the sample for each measurement performed. The evaporation losses were reduced using a solvent trap and by limiting the duration of the experiment to less than 24 h. The rheological behavior was probed both in the linear and nonlinear regime, which were accurately established by preliminary stress sweep measurements. In addition, the sinusoidal form of the response signal was checked for each run in order to verify the absence of possible slip at the wall. After the experiment, a portion of the sample was aspirated into flat x-ray capillaries in order to determine ϕ using USAXS.

D. DLS

DLS experiments were performed using a goniometer (ALV GmbH) fitted with a temperature controlled toluene bath. The incident laser wavelength was 532 nm (20 mW, diode pumped, frequency doubled Nd-YAG laser, Melles-Griot). An ALV 5000-E dual channel correlator was used to record simultaneously the intensity autocorrelation function $g^{(2)}(q,t)$. Measurements were performed at the scattering angle $\theta = 90°$ for the suspension at high volume fraction. The ensemble-averaged intensity was estimated by measuring the scattering from different parts of the sample. DLS samples were contained in cylindrical borosilicate capillaries of a diameter of 1.5 mm. The refractive indices of particles and solvent are 1.49 and 1.48, respectively. Under these conditions, the DLS measurements do not significantly suffer from multiple scattering.

III. THEORETICAL BACKGROUND

A. Static Structure

The scattering intensity $I(q)$ from a colloidal suspension of monodisperse particles can be expressed as follows:

$$I(q) = NV^2 \Delta\rho^2 P(q) S(q), \tag{1}$$

where N is the colloid number density, V is the particle volume, $\Delta\rho$ is the scattering contrast, $P(q)$ is the form factor describing the shape of the particles, and $S(q)$ is the structure factor describing the interparticle interactions.[21] In the case of a relatively dilute suspension, $S(q) \approx 1$ and $I(q)$ is governed by the shape of the scattering objects. However, colloidal particles have a size distribution which in this case can be approximately described by a Schulz size function, $f(R)$.[22] The measured $I(q)$ for a dilute suspension of PMMA particles is adequately described by a core-shell $P(q)$ function weighted by the size distribution,

$$I(q) = N \int_0^\infty P(q,R) f(R)\, dR, \tag{2}$$

$$f(R) = \left(\frac{Z+1}{R_m}\right)^{Z+1} \frac{R_m^Z}{\Gamma(Z+1)} \exp\left(-\frac{Z+1}{R_m}\right), \tag{3}$$

$$P(q,R) = (16\pi^2/9)[(\rho_{\mathrm{core}} - \rho_{\mathrm{shell}}) R_c^3 F(q,R_c) - (\rho_{\mathrm{solvent}} - \rho_{\mathrm{shell}})(R_c + t_{\mathrm{sh}})^3 F(q, R_c + t_{\mathrm{sh}})]^2, \tag{4}$$

where R_c is the size of the core particle, t_{sh} is the shell thickness, ρ_{core}, ρ_{shell}, and ρ_{solvent} are the scattering length densities of the core, shell, and solvent, respectively,[21] and $F(q,R_i)$ indicates the scattering amplitude of a sphere of radius R_i and $P(q,R_i) = F^2(q,R_i)$, with

$$F(q,R_i) = 3[\sin(qR_i) - (qR_i)\cos(qR_i)]/(qR_i)^3. \tag{5}$$

The suspensions at high volume fractions were modeled using the structure factor of HS, calculated by the Ornstein–Zernike integral equation within the Percus–Yevick (PY) approximation.[23] In the monodisperse case, the structure factor is related to ϕ and to the interparticle interaction potential, $V(r)$ through $C(q)$ which represents the Fourier transform of the pair correlation function, $C(r)$[23]

$$S(q) = 1/[1 - NC(q)]. \tag{6}$$

For a HS system N is related to ϕ as $\phi = \pi N \sigma^3/6$, where σ is the effective HS diameter ideally given by the core-shell diameter $[\sigma = 2(R_c + t_{\mathrm{sh}})]$. The PY solution at high ϕ is known to overestimate the peak of $S(q)$. Thus, $S(q)$ is calculated using a reduced volume fraction ϕ' as given by the Verlet correction,[23] i.e., $\phi' = \phi_{\mathrm{real}} - \phi_{\mathrm{real}}^2/16$.

For a polydisperse system, $S(q)$ and $P(q)$ are coupled and the effective structure factor, $S_M(q)$, involves both $S(q)$ and $P(q)$.[21,22] For the experimental HS parameters and polydispersity, $S_M(q)$ was calculated using the generalized indirect Fourier transform (GIFT) package.[24]

Above the glass transition, $I(q)$ showed an upturn at low q values that could be a signature of static heterogeneities. In this case, the excess intensity is described by an additional Lorentzian term,[25] $S_c(q)$

$$S_c(q) = \frac{I_0}{(1 + q^2\xi^2)^p}, \tag{7}$$

where ξ is proportional to the size of the heterogeneities and p is a power law exponent, with $2p \approx d_f$, the fractal dimensionality and $p=2$ for compact clusters. The total intensity including the Lorentzian term is given by:

$$I(q)=NV^2\Delta\rho^2\langle P(q)\rangle[S_M(q)+S_c(q)], \tag{8}$$

where $\langle P(q)\rangle$ is the polydisperse $P(q)$ function and in the monodisperse case, $S_M(q)\approx S(q)$.

B. Rheology

Rheological measurements were carried out both in the linear and nonlinear viscoelastic regimes. Preliminary stress sweeps have been performed in order to determine the yield threshold (τ_y) for each colloidal suspension investigated. For $\phi<\phi_G$, the frequency behavior of the elastic (G') and viscous (G'') components is typical of a viscoelastic fluid, with $G''>G'$. Their low frequency response showed the limiting power laws correspond to the classical Maxwell behavior:[26]

$$\begin{aligned} G' &\sim \omega^2 \\ G'' &\sim \omega. \end{aligned} \tag{9}$$

The glass transition was identified by the weaker frequency dependence of G' and G''.[27–29] In the glassy state, the frequency dependence of G' and G'' in the linear regime was described within the model proposed by Mason and Weitz,[29] based on MCT combined with hydrodynamic flow equations, introduced to describe the high frequency behavior:

$$\begin{aligned} G'(\omega) &= G_p+G_\sigma\left[\Gamma(1-a)\cos\left(\frac{\pi a}{2}\right)(\omega t_\sigma)^a \right.\\ &\quad \left. -B\Gamma(1+b)\cos\left(\frac{\pi b}{2}\right)(\omega t_\sigma)^{-b}\right]+G_D'(\omega), \\ G''(\omega) &= G_\sigma\left[\Gamma(1-a)\sin\left(\frac{\pi a}{2}\right)(\omega t_\sigma)^a \right.\\ &\quad \left. +B\Gamma(1+b)\sin\left(\frac{\pi b}{2}\right)(\omega t_\sigma)^{-b}\right]+G_D''(\omega)+\eta_\infty\omega. \end{aligned} \tag{10}$$

The parameters a and b were determined from the value of the critical exponent,[30] λ, derived from the MCT analysis. For the PMMA system, λ was found to be ~ 0.67 corresponding to $a=0.34$ and $b=0.69$. These exponents are slightly different from the ones for monodisperse HS, and they signify the deviation from ideal HS behavior. The amplitude B was fixed to the expected value of 0.963.[3] Thus, the free fitting parameters were the plateau modulus (G_p), the time (t_σ) which is related to frequency where the minimum of G'' is observed, the viscoelastic amplitude (G_σ), the high frequency suspension viscosity (η_∞) and G_D', calculated from the short-time diffusion coefficient.[29] Finally for glassy samples, a power law behavior of the two viscoelastic moduli was also observed for applied stress well above the yield point.

C. MCT

MCT is a first-principle theory, based on uncontrolled approximations, which predicts the glass transition in terms of an ergodic to nonergodic transition.[2,3,5] It also describes the full dynamical behavior (except for a microscopic timescale) of a system in the vicinity of the glass transition. A great advantage of the theory is that it can predict the dynamics using static information as only input.

MCT has been applied for a long time to experimental HS realizations, providing a good description of the glass transition.[6,14] However, a discrepancy of about 10% in the value of ϕ_G is usually found.[3] This discrepancy can improve either with better approximations involved in the derivation of MCT equations[31] or with a better estimate of the input $S(q)$. For this reason, in this study we apply the theory directly using the experimental structure factor, taking advantage of the extended q-range of the measurements, which allows to probe the full behavior of $S(q)$ from the compressibility limit to its final asymptotic limit of 1. For simplicity, we neglect the polydispersity of the particles and treat it as an effective monodisperse system with the experimental $S(q)$. The polydispersity effects, which in general smear out the peaks of $S(q)$ as it will be shown in the following, is not expected to have a dramatic effect on the glass transition for HS systems, apart from a shift in the transition point and some changes in the characteristic exponents. Differently, such effects would become relevant in the case of systems with additional short-ranged attractive interactions, where the mechanism for arrest is dominated by the large-q signal in $S(q)$,[32,33] for which therefore a truly multicomponent MCT treatment should be applied.

The MCT equations were solved for 2000 q values ranging from 0 to 0.533 nm^{-1}, in order to ensure a full decay to zero for the glassy nonergodicity parameters. Experimental structure factors show oscillations up to 0.3 nm^{-1}, above which we set them equal to 1, since the residual oscillations are very small.

The viscoelastic properties of the system can be calculated in the mode-coupling approximation. In particular, the stress correlation function $[C_{\sigma\sigma}(t)]$ is related to an integral over all wavevectors of the density correlation functions $f_q(t)$:[34]

$$C_{\sigma\sigma}(t)=\frac{k_BT}{60\pi^2}\int_0^\infty dq\,q^4\left[\frac{d\ln S(q)}{dq}f_q(t)\right]^2, \tag{11}$$

where $C_{\sigma\sigma}(t)$ is measured in units of k_BT/σ^3. In order to calculate elastic and viscous moduli, the stress correlation functions calculated from Eq. (11) have to be Fourier transformed

$$G(\omega)=i\omega\tilde{C}(\omega), \tag{12}$$

where $\tilde{C}(\omega)$ is the Fourier transform of $C_{\sigma\sigma}(t)$. The qualitative comparison between MCT predictions for the viscous and elastic moduli and the experimental rheological behavior will be discussed in the Results section.

D. Dynamics

In the DLS experiments, the normalized time autocorrelation function, $g^{(2)}(q,t)$, was measured[35]

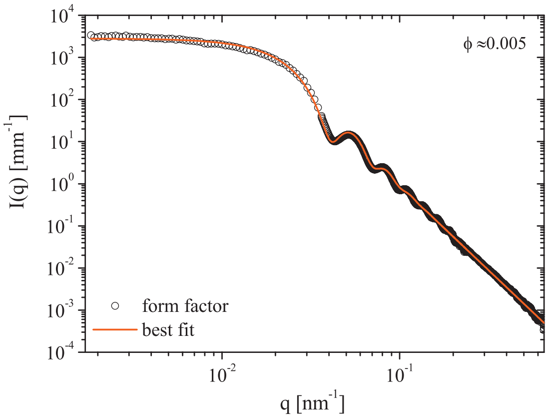

FIG. 1. SAXS intensity pattern $I(q)$ for dilute suspension of PMMA ($\phi \approx 0.005$). The solid line represents the best fit to core-shell spherical form factor weighted with Schultz size distribution; mean core radius $\bar{R}_c = 107$ nm and polydispersity 10%.

$$g^{(2)}(q,t) = \frac{\langle I(q,0)I(q,t)\rangle}{\langle I(q,0)\rangle^2}, \tag{13}$$

where $I(q,t)$ is the scattered intensity at a given wavevector q and time t. The $g^{(2)}(q,t)$ function is related to the normalized intermediate scattering function, $f(q,t)$, assuming that the system is an ergodic media[36,37]

$$g^{(2)}(q,t) = 1 + \beta |f(q,t)|^2, \tag{14}$$

where β is the coherence factor of the instrument.

For diffusive behavior, $f(q,t)$ at short times decays by an exponential function:

$$f(q,t) \sim \exp(-D_s q^2 t), \tag{15}$$

where D_s is the short-time diffusion coefficient and the corresponding relaxation time $\tau_D = 1/(D_s q^2)$. When the system becomes nonergodic, the particles are trapped in the cages formed by their neighbors and the measured $g^{(2)}(q,t)$ varies when scanning through different positions in the sample. Therefore, for nonergodic systems the time and ensemble average are no longer equivalent and $f(q,t)$ decays to a finite value, the so called nonergodicity parameter $f(q,\infty)$, which represents the frozen component of the fluctuations.[8] $f(q,t)$ and $f(q,\infty)$ are then obtained according to[36,37]

$$f(q,t) = 1 + \frac{\langle I(q)\rangle_t}{\langle I(q)\rangle_E}\left[\sqrt{1 + g_t^{(2)}(q,t) - g_t^{(2)}(q,0)} - 1\right], \tag{16}$$

$$f(q,\infty) = 1 + \frac{\langle I(q)\rangle_t}{\langle I(q)\rangle_E}\left[\sqrt{2 - g_t^{(2)}(q,0)} - 1\right], \tag{17}$$

where $\langle I(q)\rangle_t$ and $\langle I(q)\rangle_E$ indicate the time-averaged and ensemble-averaged intensity, respectively. The experimental $f(q,t)$ is directly related to the theoretical $f_q(t)$.

IV. RESULTS

A. Colloidal particles characterization

In Fig. 1, $I(q)$ from the combination of USAXS and SAXS measurements for a dilute suspension of PMMA in *cis*-decaline is shown. The data were fitted using the polydisperse core-shell spherical scattering function Eqs. (2)–(4) weighted by a Schulz size distribution (implemented in SAXS utilities program[38]) with mean core radius $\bar{R}_c$ of 107 nm and polydispersity of 10%. The shell thickness was fixed to 10 nm, on the basis of the size of the stabilizer. The volume fraction evaluated from the absolute intensity level is $\approx$0.005.

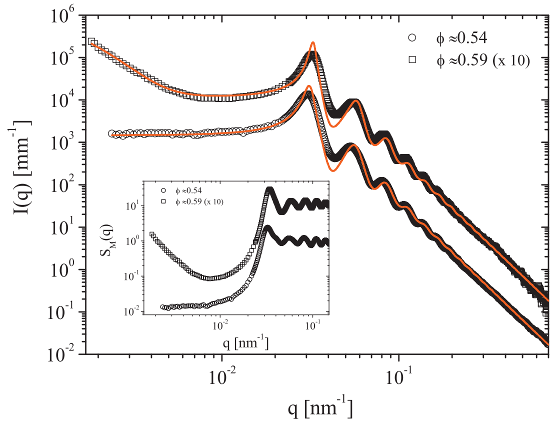

FIG. 2. Combined USAXS and SAXS intensities and corresponding fits to Eqs. (1) and (8) (solid lines) for PMMA suspensions of $\phi \approx 0.54$ (open circles) and $\phi \approx 0.59$ (open squares), respectively. The effective σ was 225 nm. USAXS and SAXS intensities were merged at $q \approx 0.025$ nm^{-1}. Inset presents the corresponding experimental $S_M(q)$ derived from $I(q)$. For better visibility both the absolute $I(q)$ and the corresponding $S_M(q)$ of higher ϕ are multiplied by 10.

B. Microstructure

The evolution of the structure of PMMA suspension from the fluid to glassy state is shown in Fig. 2. The fitted line for $I(q)$ in the fluid state results from Eq. (1) with the $P(q)$ function in Fig. 1 and a monodisperse HS $S(q)$ calculated using an effective diameter, σ of core-shell particles. However, the effective HS diameter was found to be slightly smaller than the size calculated from the form factor analysis in both the fluid and glassy states [$\sigma \approx 225$ nm], with $\sigma = 2(R_c + t_{sh}) - \delta$ due to possible interpenetration of particle shells at these high volume fractions. In the glassy state, in addition to HS structure, an upturn of intensity was observed at low q values. This is attributed to large scale heterogeneities in the sample and the total intensity is described by Eq. (8). The polydispersity of the particles is known to influence not only the $P(q)$ function, but also $S(q)$. The deviation between the data and the fits is a consequence of the use of monodisperse $S(q)$. The polydisperse structure factors, $S_M(q)$ deduced from $I(q)$ in Fig. 3(a) and the experimental $P(q)$ are shown in Fig. 3(b). The transition from fluid to glassy state is monitored by the shift in the first structure factor peak toward higher q values and by the increase in its height. In Fig. 3(c) we show a comparison between the experimental data for the volume fraction $\phi \approx 0.54$, and $S(q)$ calculated via PY closure for the monodisperse HS case, as well as the $S_M(q)$

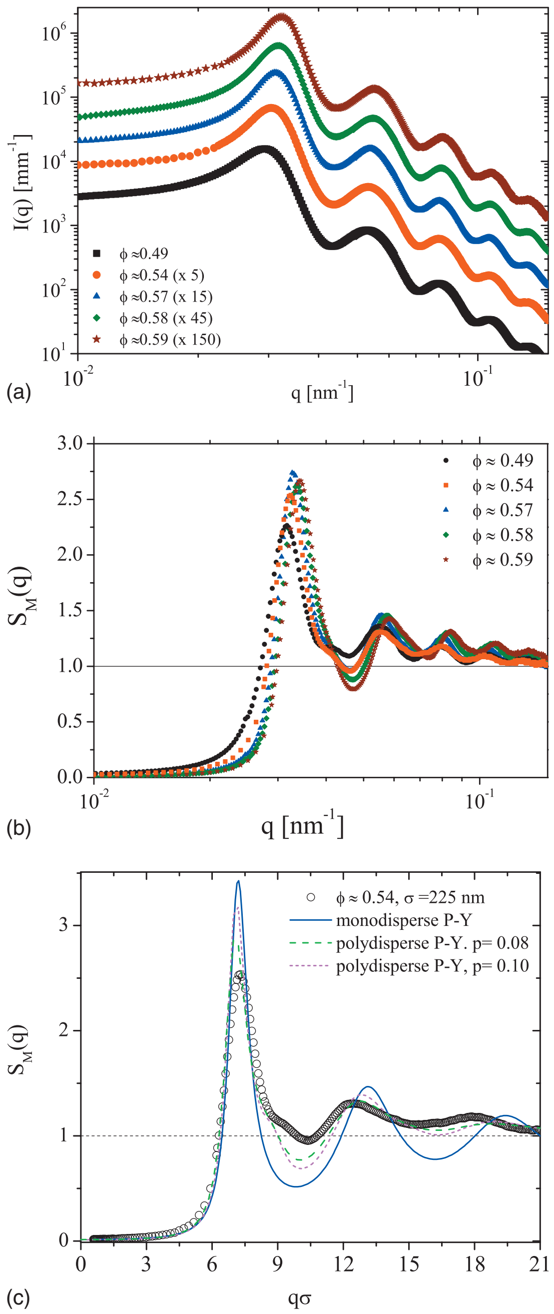

FIG. 3. (a) Measured $I(q)$ for different volume fractions of PMMA in *cis*-decaline. For clarity, the absolute intensities are multiplied by the factor indicated in the legend. (b) The evolution of $S_M(q)$ deduced from the measured $I(q)$ in the liquid to the glassy states. (c) $S(q)$ corresponding to $\phi \approx 0.54$. The lines indicate the corresponding simulation of polydisperse $S_M(q)^{\mathrm{PY}}$, for $\sigma = 225$ nm and polydispersity in size distribution from 0 up to 10%.

obtained using the GIFT for two different values of polydispersities around the experimental one. While the inclusion of polydispersity goes in the direction of improving the data description, it remains rather unsatisfactory. This suggests that PMMA particles deviate from polydisperse HS behavior at the microstructural level. A further improvement may be obtained using the approximation developed by Gazzillo and Giacometti,[39] but the need for a precise description of $S(q)$ even at large wavevectors for the use of MCT prompted us to rely exclusively on the experimental data.

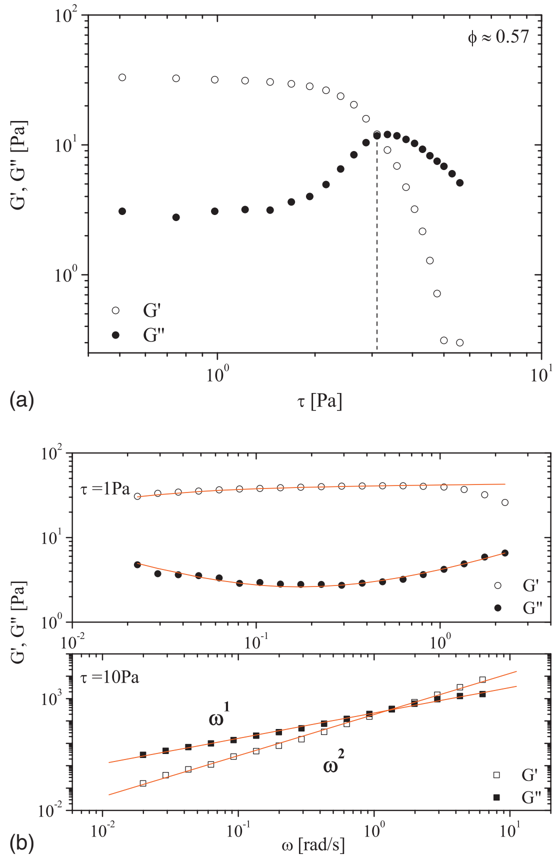

FIG. 4. (a) Rheological measurements at a frequency of $\omega = 0.628$ rad/s showing G' (open symbols) and G'' (filled symbols) as a function of the applied stress τ for PMMA suspension of $\phi \approx 0.57$. The dashed line indicates the yield point, τ_y. (b) The frequency dependence of the storage G' and loss G'' modulus for PMMA suspension of $\phi \approx 0.57$, showing glassy ($\tau = 1$ Pa) and fluid behavior ($\tau = 10$ Pa), respectively, as a function of the applied stress. The solid lines represent the best fits to Eqs. (10) and (9) for the glassy and fluid states, respectively.

C. Rheology

In order to characterize the glass transition, we performed bulk rheology investigations. Figure 4(a) depicts the typical yielding behavior of the sample and the corresponding elastic (G'), and the viscous (G'') components as a function of the applied stress (τ) for PMMA suspension of $\phi \approx 0.57$, at $\omega = 0.628$ rad/s. As previously reported,[40] G'' shows a peak near the yield point ($\tau \approx 3$ Pa), typical feature observed in soft glassy materials,[27] which is a sign of the structural rearrangements occurring in the system. The variation in the elastic and viscous components below ($\tau = 1$ Pa) and well above ($\tau = 10$ Pa) the yield point (τ_y) is shown in Fig. 4(b). At low stress values, G' and G'' show only a weak frequency dependence demonstrating the glassy behavior of the sample,[27] while the application of large enough stress well above the yield stress causes the glass to flow and the terminal behavior is approached ($G' \sim \omega^2$, $G'' \sim \omega$). At $\tau = 1$ Pa the model proposed by Mason and Weitz[29]describes the experimental data when the elastic component is the dominant one. The fast dynamics involving the hydrodynamic interaction has been independently obtained from DLS measurements and incorporated in the frequency dependence of the viscoelastic modulus. The dependence of the

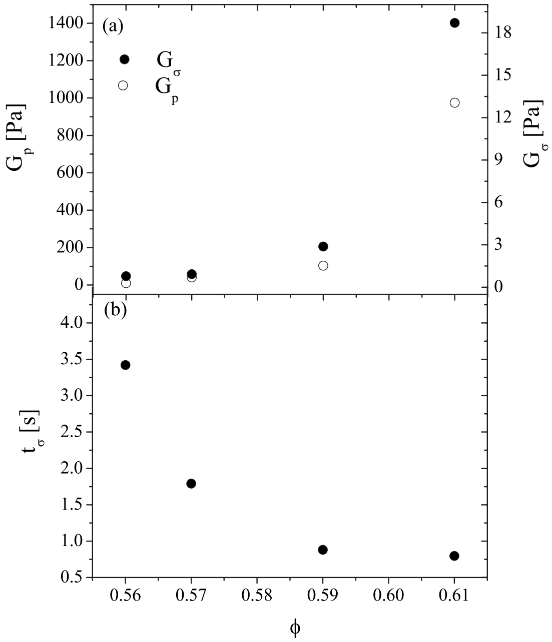

FIG. 5. Volume fraction dependence of the parameters (a) G_p, G_σ, and (b) t_σ obtained from the fit to Eq. (10) above ϕ_G.

fitting parameters (G_p, G_σ, and t_σ) on the volume fraction is shown in Fig. 5. G_p and the viscoelastic amplitude G_σ increase considerably with ϕ, in analogy with similar results reported on different PMMA samples.[40,41]

In Fig. 6 the stress correlation function $C_{\sigma\sigma}(t)$ calculated within MCT [Eq. (11)] using the experimental $S(q)$ as input, is shown for three different volume fractions, above and below the predicted MCT transition. Recently, a comparison between the computer simulations and MCT results for $C_{\sigma\sigma}(t)$ for both HS and attractive glasses[42,43] has been reported, showing that the maximum contribution for the integral determining $C_{\sigma\sigma}(t)$ in Eq. (11) occurs at a well-specified wavevector, which for HS glasses is found to be close to the first peak of $S(q)$. This means that the relaxation of the stress correlation is controlled by the same length-scale controlling arrest at the local level. Here, we provide a comparison between $C_{\sigma\sigma}(t)$ and the (squared) density correlator $f_q^2(t)$ at the main peak of $S(q)$ (i.e., $q\sigma \simeq 7.5$). However, we find that this choice of wavevector does not describe well the long-time relaxation of $C_{\sigma\sigma}(t)$, while instead a very good agreement is obtained if we consider a larger wavevector, i.e., $q\sigma=9.5$, which is actually close to the first minimum of $S(q)$. The origin of this discrepancy may be attributed to a combination of factors including the size polydispersity and softness of interaction potential. However, we want to stress that, in agreement with the simulation results of Puertas *et al.*,[42,43] a dominant length-scale contributing to the integral appearing in Eq. (11) is responsible for describing the full long-time behavior of $C_{\sigma\sigma}(t)$ also in our particular case.

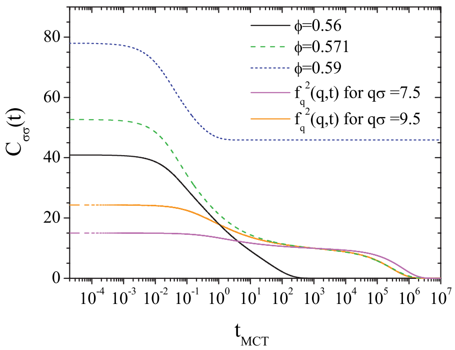

FIG. 6. MCT predictions for the stress correlation function $C_{\sigma\sigma}(t)$ for the volume fractions of 0.56, 0.571, and 0.59. The squared density correlation functions, $f_q^2(t)$, arbitrarily scaled in amplitude in order to overlap the long-time behavior, calculated for $q\sigma=7.5$ and 9.5 are also shown.

Figure 7 I and II show the behavior of the elastic G' and viscous G'' moduli from MCT calculations using $S_M(q)$ data in Fig. 3(b). For a comparison, Fig. 7 III and IV illustrate the corresponding experimental data as a function of increasing volume fraction. Experimentally, we observe that the fluid state is located below $\phi \approx 0.56$; at the volume fraction of 0.55, fluidlike behavior is indeed observed over the full range of stress investigated. To track more precisely the location of the predicted MCT transition, we have also interpolated data in the range $0.57 < \phi < 0.58$. Theoretically, we observed the ergodic to nonergodic transition (ϕ_G) around $\phi \gtrsim 0.571$, a value quite close to the experimental one. Hence, the direct use of experimental $S(q)$ significantly improved the location of the MCT transition, despite the fact that we used a monodisperse approximation for the system. The MCT exponent parameter λ is found to be ≈0.67, quite close to the typical HS one.[3]

Comparing the theoretical curves for G' and G'' with the experimental ones over the same frequency window, we observe a qualitative agreement between the MCT and the experimental data, though a significant underestimation of both moduli is found similar to that observed in the comparison with simulations reported in Ref. 43. These findings suggest that the mode-coupling approximation for the stress correlation function, used to derive Eq. (11) is too severe, missing out some substantial contributions to the stress relaxation, though its functional form appears to be correctly predicted. The value of the glass transition (ϕ_G) from MCT is also reported in Fig. 8, together with the dependence on ϕ of the yield stress τ_y, obtained from the rheological investigation.

To complete the comparison between MCT and experiments, in Fig. 9 we report the experimental and the predicted $f(q,t)$ from MCT for various volume fractions using the experimental $S_M(q)$. The microscopic time has been chosen to be ≈3.5 ms, in order to match the experimental time window. We observe a quite remarkable agreement between the two sets of curves, both in terms of the growth of the relaxation time, of the functional form of the relaxation and also on the value of the long-time plateau, considering that we tried to compare sufficiently close values of ϕ compatibly with the available experimental measurements. We note that the two sets of curves correspond to slightly different values of the wavevector ($q=0.0247$ nm^{-1} in experiments versus $q=0.027$ nm^{-1} for MCT), such a shift being applied in order to optimize the agreement, and again probably resulting from the fact that the real system is polydisperse while we use a monodisperse theoretical treatment.

Finally, we have attempted similar analysis using the

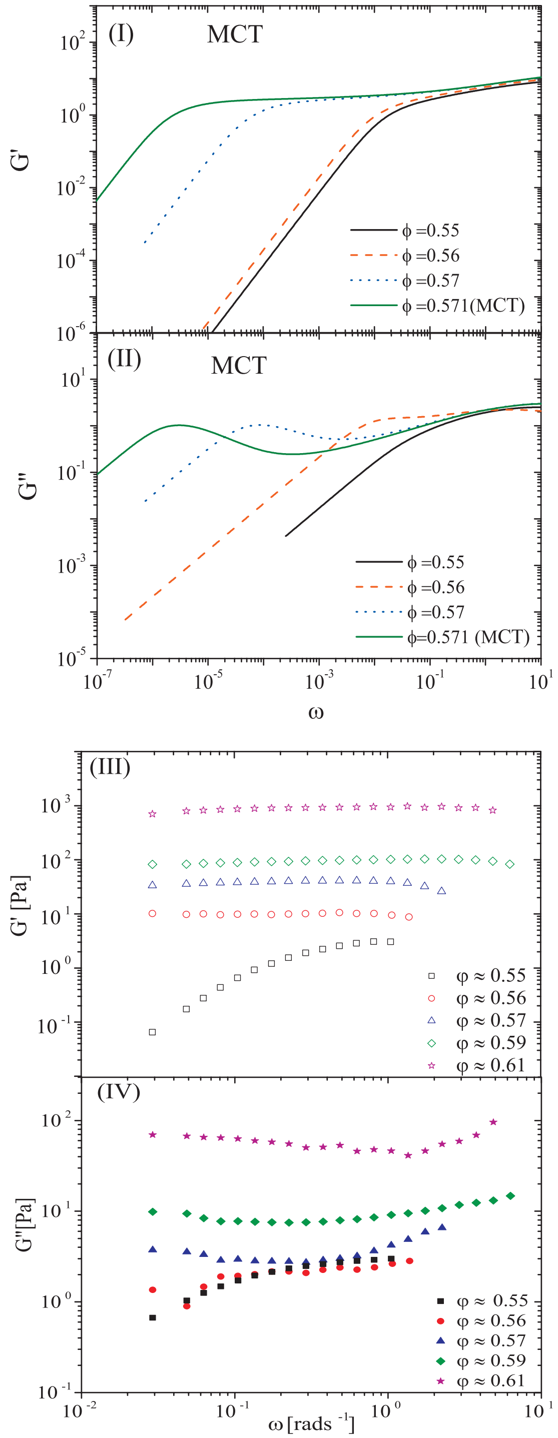

FIG. 7. MCT predictions for G' (I) and G'' (II) calculated from the experimental $S(q)$ of PMMA suspensions at different volume fractions. The MCT transition is also indicated in the graphs. Experimental elastic G' (III) and shear viscous modulus G'' (IV) as a function of the frequency for PMMA suspensions at different volume fractions.

experimental $S(q)$ data for a model attractive colloidal glass system consisting of silica particles suspended in a marginal solvent (n-dodecane).[44] However, in this case the smearing of high q oscillations in the $S_M(q)$ due to polydispersity led to a suppression of the attractive glass transition. In other words, experimental $S(q)$ and one component MCT is not sufficient to predict an attractive glass transition and full multicomponent analysis is required.

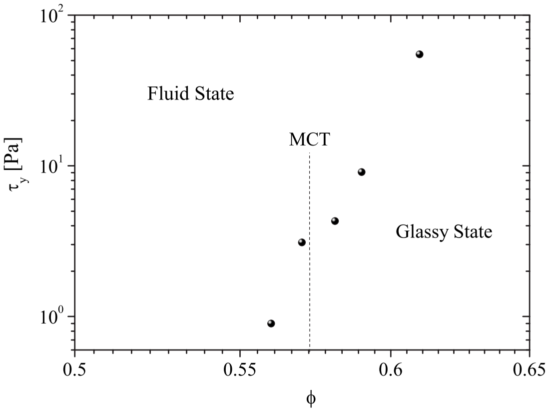

FIG. 8. The yield stress (τ_y) as a function of the volume fraction for concentrated suspension of PMMA particles. The dashed line indicates the MCT prediction for the fluid to glass transition.

V. DISCUSSION

The static structure, dynamics, and rheological behavior of a model colloidal system was studied over a concentration range in the vicinity of the glass transition. The model system presented here is convenient for testing the theoretical predictions, as well as for quantitative scattering studies. The combination of SAXS and USAXS provided quantitative $S(q)$ data which could be used as input to MCT. The volume fraction is often an uncertain parameter in colloid science. As shown here, the volume fraction can be deduced *in situ* using the $S(q)$ together with the absolute scale of $I(q)$. However, it has been shown that $S_M(q)$ deviates appreciably from theoretical polydisperse models. These deviations from the ideal HS behavior were observed at high volume fractions, which could have influenced the exact location of ϕ_G. MCT has been shown to be very sensitive to structural features on the nearest-neighbor length scale (i.e., the structure factor peak values) when predicting the arrested state.[45] Nevertheless, in the case of HS, the use of the experimental $S(q)$ as input for MCT calculations seems to be able to predict quite accurately the location of the glass transition, without requiring

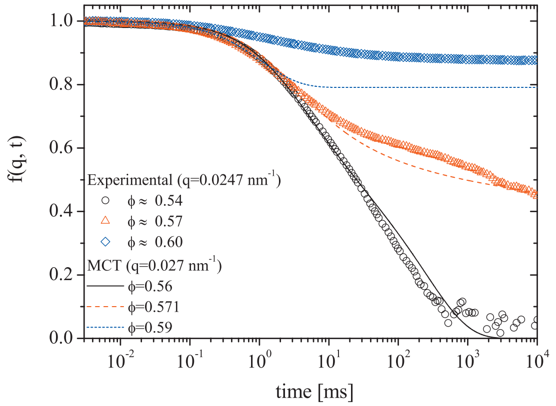

FIG. 9. Normalized intermediate scattering functions $f(q,t)$ at $q = 0.0247\ \text{nm}^{-1}$ for PMMA suspension of $\phi \approx 0.54$, 0.57 and 0.60. The direct comparison with the theoretical behavior from MCT calculations at $q = 0.027\ \text{nm}^{-1}$ is also shown. Note that the temporal scale of MCT has been rescaled to match the experimental time window ($t_{\text{MCT}} \approx 3.5$ ms).

the inclusion of higher order coupling terms in the MCT kernel.

In the glassy state an intense low-q upturn in the scattering data seems to suggest the presence of static heterogeneities which disappears upon shearing. We note that, however, this upturn is irrelevant for determining the MCT transition, which was found to happen at a certain ϕ_G independently of whether such low-q increase was included or not in the calculations. The fluid to glass transition was accurately detected experimentally from the frequency dependence of the elastic and viscous components of the shear modulus. In the fluid state, the terminal regime was observed, while above the glass transition the model of Mason and Weitz[29] was found to satisfactorily describe the frequency dependence of the shear moduli.

The MCT calculations qualitatively reproduce the experimental rheological behavior of the repulsive glass. Better agreement was found for the elastic than the viscous component, when comparing the same frequency window, but in general the amplitudes of the moduli appear to be rather low. In contrast to previous rheological studies on flow behavior of colloidal thermosensitive core-shell particles,[15,16] we did not achieve a complete quantitative description of our experimental rheological parameters by the theory. The density relaxation is however quite well described by the theory as compared from DLS measurements, in agreement with previous experimental studies of HS glasses.[6]

VI. CONCLUSION

In this article we have reported a study of the microstructure and rheology of a model colloidal system in the proximity of the glass transition. The combination of USAXS and SAXS allowed a precise determination of the $S(q)$, from the compressibility limit to its final high-q limit of 1. The effective ϕ was estimated by the modeling of $S(q)$ together with the absolute scale of the scattering intensity. Although, PMMA particles in *cis*-decaline are considered as a model HS system, significant deviation from the PY model structure factor is noticed at higher q ranges. This departure from ideal HS microstructure could be at the origin of the higher ϕ_G observed in this system.

The rheological properties were compared with those derived from MCT using the experimental structure factors as input to the theory. The experimental behavior of the viscoelastic moduli satisfactorily reproduced the predicted ones, approaching the glass transition. While there is a qualitative agreement with the viscoelastic properties calculated by MCT, the direct comparison between theory and experiment suggests that a one-to-one correspondence could not be achieved. The use of a modified version of MCT, including explicitly shearing effects in the memory kernel,[15,16,46,47] is probably the route to be pursued in future investigations.

ACKNOWLEDGMENTS

We thank P. Panine for technical support for rheometry and A.B. Schofield for help in the synthesis of PMMA particles. We also thank M. Ballauff, P. Pusey, A. Giacometti, and F. Sciortino for helpful discussions. The European Synchrotron Radiation Facility is acknowledged for the financial support and the provision of synchrotron beam time. E.Z. acknowledges support from EU Marie Curie Research and Training Network Grant No. MRTNCT-2003-504712 and NoE SoftComp Grant No. NMP3-CT-2004-502235.

[1] P. N. Pusey, in *Liquids, Freezing and Glass Transition*, edited by J. P. Hansen, D. Levesque, and J. Zinn-Justin (North-Holland, Amsterdam, 1991), p. 787.

[2] W. Götze, in *Liquids, Freezing and Glass Transition*, edited by J. P. Hansen, D. Levesque, and J. Zinn-Justin (North-Holland, Amsterdam, 1991), p. 287.

[3] W. Götze and L. Sjogren, Rep. Prog. Phys. **55**, 241 (1992).

[4] F. Sciortino and P. Tartaglia, Adv. Phys. **54**, 471 (2005).

[5] U. Bengtzelius, W. Götze, and A. Sjölander, J. Phys. C **17**, 5915 (1984).

[6] W. van Megen, S. M. Underwood, and P. N. Pusey, Phys. Rev. Lett. **67**, 1586 (1991).

[7] L. Fabbian, W. Götze, F. Sciortino, P. Tartaglia, and F. Thiery, Phys. Rev. E **59**, R1347 (1999).

[8] J. Bergenholtz and M. Fuchs, Phys. Rev. E **59**, 5706 (1999).

[9] K. A. Dawson, G. Foffi, M. Fuchs, W. Goetze, F. Sciortino, M. Sperl, P. Tartaglia, T. Voigtmann, and E. Zaccarelli, Phys. Rev. E **63**, 011401 (2000).

[10] K. N. Pham, A. M. Puertas, J. Bergenholtz, S. U. Egelhaaf, A. Moussaïd, P. N. Pusey, A. B. Schofield, M. E. Cates, M. Fuchs, and W. C. K. Poon, Science **296**, 104 (2002); K. N. Pham, S. U. Egelhaaf, P. N. Pusey, and W. C. K. Poon, Phys. Rev. E **69**, 011503 (2004).

[11] A. M. Puertas, M. Fuchs, and M. E. Cates, Phys. Rev. Lett. **88**, 098301 (2002).

[12] G. Foffi, K. A. Dawson, S. V. Buldyrev, F. Sciortino, E. Zaccarelli, and P. Tartaglia, Phys. Rev. E **65**, 050802 (2002).

[13] E. Zaccarelli, J. Phys.: Condens. Matter **19**, 323101 (2007).

[14] Th. Voigtmann, A. M. Puertas, and M. Fuchs, Phys. Rev. E **70**, 061506 (2004).

[15] J. Crassous, R. Régisser, M. Ballauff, and N. Willenbacher, J. Rheol. **49**, 851 (2005).

[16] J. Crassous, M. Siebenbürger, M. Ballauff, M. Drechsler, O. Henrich, and M. Fuchs, J. Chem. Phys. **125**, 204906 (2006).

[17] M. Zackrisson, A. Stradner, P. Schurtenberger, and J. Bergenholtz, Phys. Rev. E **73**, 011408 (2006).

[18] V. Kobelev and K. S. Schweizer, J. Chem. Phys. **123**, 164903 (2005).

[19] V. Gopalakrishnan and C. F. Zukoski, Langmuir **23**, 8187 (2007).

[20] T. Narayanan, O. Diat, and P. Boesecke, Nucl. Instrum. Methods Phys. Res. A **467**, 1005 (2001).

[21] T. Narayanan, in *Soft Matter Characterization*, edited by R. Borsali and R. Pecora (Springer, New York, 2008), Vol. II, p. 899.

[22] M. Kotlarchyk and S.-H. Chen, J. Chem. Phys. **79**, 2461 (1983).

[23] R. Klein and B. D'Aguanno, in *Light Scattering: Principles and Development*, edited by W. Brown (Clarendon, Oxford, 1996), p. 30.

[24] G. Fritz, A. Bergmann, and O. Glatter, J. Chem. Phys. **113**, 9733 (2000).

[25] M. Sztucki, T. Narayanan, G. Belina, A. Moussaïd, F. Pignon, and H. Hoekstra, Phys. Rev. E **74**, 051504 (2006).

[26] R. G. Larson, *The Structure and Rheology of Complex Fluids* (Oxford University, New York, 1998).

[27] P. Sollich, Phys. Rev. E **58**, 738 (1998).

[28] S. Ramakrishnan, Y. L. Chen, K. S. Schweizer, and C. F. Zukoski, Phys. Rev. E **70**, 040401 (2004).

[29] T. G. Mason and D. A. Weitz, Phys. Rev. Lett. **75**, 2770 (1995).

[30] W. Götze, J. Phys.: Condens. Matter **2**, 8485 (1990).

[31] J. Wu and J. Cao, Phys. Rev. Lett. **95**, 078301 (2005).

[32] F. Sciortino, P. Tartaglia, and E. Zaccarelli, Phys. Rev. Lett. **91**, 268301 (2003).

[33] E. Zaccarelli, G. Foffi, K. A. Dawson, S. V. Buldyrev, F. Sciortino, and P. Tartaglia, J. Phys.: Condens. Matter **15**, S367 (2003).

[34] G. Nagele and J. Bergenholtz, J. Chem. Phys. **108**, 9893 (1998).

[35] R. Pecora, *Dynamic Light Scattering. Applications of Photon Correlation Spectroscopy* (Plenum, New York, 1985).

[36] A. Moussaïd, P. N. Pusey, J. J. M. Slot, and J. G. H. Joosten, Macromolecules **32**, 3774 (1999).

[37] P. N. Pusey and W. Van Megen, Physica A **157**, 705 (1989).

[38] M. Sztucki and T. Narayanan, J. Appl. Crystallogr. **40**, S459 (2007).
[39] D. Gazzillo and A. Giacometti, J. Chem. Phys. **113**, 9837 (2000).
[40] K. N. Pham, G. Petekidis, D. Vlassopoulos, S. U. Egelhaaf, P. N. Pusey, and W. C. K. Poon, J. Rheol. **52**, 649 (2008).
[41] N. Koumakis, A. B. Schofield, and G. Petekidis, Soft Matter **4**, 2008 (2008).
[42] A. M. Puertas, E. Zaccarelli, and F. Sciortino, J. Phys.: Condens. Matter **17**, L271 (2005).
[43] A. M. Puertas, C. De Michele, F. Sciortino, P. Tartaglia, and E. Zaccarelli, J. Chem. Phys. **127**, 144906 (2007).
[44] T. Narayanan, M. Sztucki, G. Belina, and F. Pignon, Phys. Rev. Lett. **96**, 258301 (2006).
[45] M. J. Greenall, Th. Voigtmann, P. Monthoux, and M. E. Cates, Phys. Rev. E **73**, 050501R (2006).
[46] M. Fuchs and M. E. Cates, Phys. Rev. Lett. **89**, 248304 (2002).
[47] M. Fuchs and M. E. Cates, Faraday Discuss. **123**, 267 (2003).